Laser-initiated magnetization reversal and correlated morphological effects visualized with in situ Fresnel transmission electron microscopy

Karl B. Schliep, Jun-Yang Chen, Mo Li, Jian-Ping Wang, and David J. Flannigan

Phys. Rev. B **94**, 104407 — Published 6 September 2016

DOI: 10.1103/PhysRevB.94.104407

Laser-Initiated Magnetization Reversal and Correlated Morphological Effects Visualized with *In Situ* Fresnel Transmission Electron Microscopy

Karl B. Schliep[1], Jun-Yang Chen[2], Mo Li[2], Jian-Ping Wang[2], and David J. Flannigan[1,*]

[1]*Department of Chemical Engineering and Materials Science, University of Minnesota, 421 Washington Avenue SE, Minneapolis, Minnesota 55455, USA*

[2]*Department of Electrical and Computer Engineering, University of Minnesota, 200 Union Street SE, Minneapolis, Minnesota 55455, USA*

[*]Author to whom correspondence should be addressed.
E-mail: flan0076@umn.edu
Phone: +1 (612) 625-3867
Fax: +1 (612) 626-7246

Abstract: Laser-initiated switching of magnetization direction in ferrimagnetic rare-earth transition metal (RE-TM) alloys – whether laser-induced or photothermal via compensation point – is being vigorously pursued owing to the promise of extending operating frequencies of magnetic devices into the terahertz regime. Despite intense interest, however, the effects of repeated laser exposure on the film structure and subsequent switching behavior has yet to be investigated. In order to better understand the correlated effects of femtosecond (fs) laser irradiation on both the magnetic response and photoinduced morphological variations of RE-TM alloys, we performed *in situ* Fresnel transmission electron microscopy (TEM) on $Tb_{23}Co_{77}$ thin films with Ta protecting layers. Via optical access to the specimen in a modified TEM, we irradiated the thin films *in situ* with both individual and series of fs optical pulses, and correlated laser-induced changes in magnetic domain-wall formation and growth with photothermal crystal formation and accompanying pinned magnetic sites. We find that, for a range of applied laser

fluences and numbers of individual pulses, several distinct regions are formed displaying varied magnetic behavior (switchable, non-switchable, demagnetized) and morphological features (small-to-large crystal-grain variations). Through a series of systematic studies, we quantified these linked magnetic and morphological properties as a function of laser fluence, number of pulse-train cycles, and number of individual fs laser pulses and the duration between each. Our results show how the sensitive connection between magnetic behavior and morphological structure can emerge in magneto-optic experiments across several parameters, thus illustrating the need for rigorous characterization so that potential operating regimes may be universally identified.

INTRODUCTION

Amorphous ferrimagnetic rare-earth transition-metal (RE-TM) alloys (*e.g.*, TbCo, TbFeCo, GdFeCo, *etc.*) have garnered a great deal of attention as promising material candidates for optically-recordable magnetic-memory storage [1-3]. In thin films of these alloys, as well as several other material types and architectures, magnetization reversal can be induced on the ultrafast timescale by irradiation with femtosecond (fs) laser pulses [4,5]. For magnetic heterostructures [6], nanopillar-type architectures [7], and ultimately devices [8], this is especially attractive because operating parameters would be limited only by the intrinsic switching time of the specimen without reliance on an external magnetic field. In addition to this, photothermal-assisted switching is arising as a promising means, complementary to the all-optical method, to induce fs switching and to increase areal densities [9-12]. As such, implementation of materials and architectures displaying such phenomena, in combination with the now robust generation of fs optical pulses with compact solid-state lasers, could potentially extend operational frequencies into the terahertz (10^{12} to 10^{14} s^{-1}) regime [1,13].

Since the first demonstration of ultrafast single-laser-pulse demagnetization in Ni [14] and later the fully-deterministic magnetization switching in GdFeCo [4], ultrafast magnetization dynamics have been vigorously studied, and a battery of techniques [*e.g.*, time-resolved magneto-optic Kerr-effect (MOKE) microscopy, photoelectron-emission electron microscopy, and ultrafast X-ray diffraction] have been used to probe the origins and behavior of the phenomenon [4,6,15-17]. However, despite intense activity, little attention has been paid to the physical effects of laser irradiation on film structure and morphology and the implications for impact on device operation. While theoretical operating limits of such devices would be dictated by optical switching times and laser repetition rates, processes occurring over much longer

60 timescales, such as the accumulation of photothermal energy and resulting effects on film
61 morphology and composition, may actually be the ultimate limiting factors in practice. For
62 multi-sublattice films, such thermal effects may initially be heterogeneously distributed owing to
63 nanoscale variation in optical properties, thus potentially leading to morphological and
64 compositional changes that are deleterious to robust operation, depending upon diffusion rates
65 and ablation thresholds. The issue is further complicated by noting the large experimental
66 parameter space containing many variables associated with both the fs laser system (*e.g.*,
67 fluence, spot size, pulse duration, repetition rate, *etc.*) and the thin-film specimen (*e.g.*,
68 composition, thickness, capping-layer properties, *etc.*) [15,18,19].

69 In order to better understand the above-discussed issues, we have studied the effects of
70 fs-laser irradiation on correlated magnetic and morphological structures of amorphous TbCo thin
71 films by way of direct visualization with combined Fresnel imaging and *in situ* transmission
72 electron microscopy (TEM). While GdFeCo has received a good deal of attention with respect
73 to the study of laser-initiated magnetic switching, its relatively weak perpendicular magnetic
74 anisotropy and low coercivity are undesirable for many potential device applications.
75 Accordingly, alloys containing Tb are increasingly receiving attention owing to the large orbital
76 angular momentum contribution to the magnetization [20]. Here, the effects of irradiating thin
77 amorphous films of TbCo with individual and series of fs laser pulses was monitored *in situ*, and
78 correlated changes in magnetic-domain size, magnetic reversibility, and degree of crystalline
79 order were determined. From bright-field Fresnel images, domain-wall formation and
80 expansion, as well as thermally-induced crystal growth and accompanying pinned magnetic sites,
81 were observed and quantified as a function of incident laser fluence. Following laser irradiation,
82 both switchable and fixed magnetic domains were formed, in addition to small-to-large grain

83 morphological variation; the magnetically-fixed regions remained largely unchanged after
84 application of switching fields up to 1.2 T, as generated by the objective lens of the TEM.
85 Further, the onset and growth of fixed domains were imaged as a function of the number of
86 pulse-train cycles and compared to the size of the switchable area. Variations in laser-initiated
87 magnetic regions were also spatially mapped as a function of the number of laser pulses and the
88 duration between each.

89

90 **METHODS**

91 **Preparation and characterization of TbCo specimens.** Thin films of TbCo were
92 deposited directly onto amorphous silicon nitride (Si_3N_4) membranes (TEMwindows.com) by
93 sputtering elemental Tb and Co (Testbourne Ltd.) using a six-target Shamrock UHV system
94 operated at a base pressure of at most 10^{-10} bar. The films were capped with thin layers of Ta in
95 order to stave off oxidation. As deposited, the specimens consisted of Si_3N_4(15 nm)/Ta(4
96 nm)/$Tb_{23}Co_{77}$(20 nm)/Ta(4 nm). The composition of the TbCo layer was determined with
97 Rutherford backscattering spectrometry, and film thicknesses were measured using X-ray
98 reflectivity (except for that of Si_3N_4, which is quoted from the manufacturer). A vibrating-
99 sample magnetometer was used to verify the out-of-plane perpendicular orientation of the
100 magnetization vector and determine the compensation temperature of the TbCo film [21].

101 ***In situ* laser irradiation and Fresnel imaging.** Representative bright-field and Fresnel
102 images of as-prepared films and a photo-initiated domain-wall structure arising from *in situ* laser
103 irradiation are shown in Fig. 1. Note that the observed magnetization reversal reported here
104 could arise from either all-optical or photothermally-assisted mechanisms. Fresnel imaging (*i.e.*,
105 imaging of magnetic domain walls) can be done with a conventional TEM via de-excitation of

106 the objective lens and use of the intermediate lenses to over/underfocus the image. In the
107 absence of the relatively strong objective-lens field, incoming swift electrons experience a
108 Lorentz force arising from the intrinsic magnetism of the thin-film specimen. Depending upon
109 the magnetization orientation in the film, electrons are deflected at the domain walls such that
110 their trajectories either converge or diverge along paths leading to the detector. This produces
111 light and dark features in the defocused bright-field images, respectively, that are representative
112 of the domain-wall shape and location, as well as the in-plane magnetization direction [22]. The
113 observed domain-wall width is a function of the defocus value and the TEM specimen-dependent
114 thickness and anisotropy energy. For the defocus values used here, the fringes have a width of
115 0.73 μm full-width at half-maximum (FWHM).
116

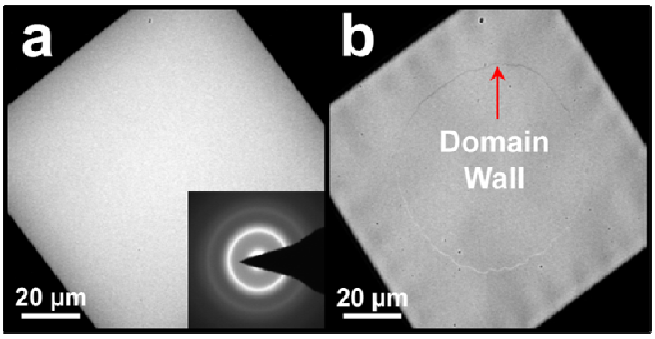

117

118 FIG. 1. Representative bright-field and Fresnel images arising from *in situ* laser irradiation. (a)
119 An in-focus bright-field image with an inset parallel-beam electron diffraction pattern obtained
120 from the film illustrating the small-grained morphology. (b) A defocused Fresnel image of a
121 roughly circular domain wall (a portion of which is labeled) formed with *in situ* laser irradiation.
122

123 Fresnel imaging of *in situ* laser irradiation was performed with a modified TEM (Tecnai
124 Femto, FEI Company) interfaced with a fs laser system (PHAROS, Light Conversion). Laser
125 irradiation of the specimen [wavelength = 515 nm, polarization = linear, pulse duration = 270 fs

126 FWHM, spot size on specimen = 100 μm FWHM; variable repetition rate, irradiation time, and
127 fluence; detailed throughout the text] was achieved via an optical window and steering-mirror
128 assembly externally situated adjacent to the TEM goniometer. In general, fs pulses are trained
129 onto the specimen region of interest by iterative beam alignment and focusing of the optical
130 elements. In this work, Fresnel imaging was conducted with either 0 or 6% objective-lens
131 excitation (*i.e.*, either completely powered down or at typical low-magnification settings,
132 respectively). In order to test the reversibility of the laser-irradiated specimen regions, and to re-
133 establish the magnetization direction when desired, the objective-lens excitation was increased to
134 88%. At these lens-excitation values (0, 6, and 88%), the magnetic field was measured at the
135 specimen location to be 10 mT, 90 mT, and 1.2 T, respectively. It is important to note that few
136 reports document the use of this kind of instrumentation for the *in situ* study of laser-initiated
137 magnetization changes [23,24], though other advances are aimed at increasing such capabilities
138 [25-27]. Further, application of these particular methods to specifically image magneto-optic
139 phenomena and correlated morphological effects has not yet been reported, though other means
140 have indeed been employed [28].
141

142 **RESULTS AND DISCUSSION**

143 Fig. 2 shows the result of irradiating a thin-film specimen *in situ* with a train of fs laser
144 pulses. Prior to laser irradiation and Fresnel imaging, the specimen magnetization orientation
145 was set by exciting the objective lens to 88%, thus creating a 1.2-T aligning field. At focus and
146 with 6% objective-lens excitation (*i.e.*, low magnification), bright-field images of the pre-
147 irradiated amorphous films show weak contrast with no discernible features aside from the
148 interface of the electron-transparent region and the thick (electron-opaque) underlying silicon

substrate [Fig. 1(a)]. After irradiation with a train of linearly-polarized fs pulses (20-kHz repetition rate, fluence = 3.8 mJ/cm^2) for several seconds, however, strong contrast arising from magnetization pinned at photothermally-induced crystal-nucleation sites was observed at large defocus values [Fig. 2]. Three distinct regions can be identified in the resulting Fresnel images: (1) a densely-nucleated nanocrystalline region spanning approximately 20 μm across the center of the laser-focal spot, (2) a sparsely-nucleated region extending radially outward approximately 10 μm from the point of cessation of the center region and having a roughly spoke-like pattern, and (3) the remaining undamaged region consisting of weak contrast and, when acquired out of focus, a magnetically-switchable region outlined by a domain wall. The general shape and size of the pattern is commensurate with the incident Gaussian pulse train.

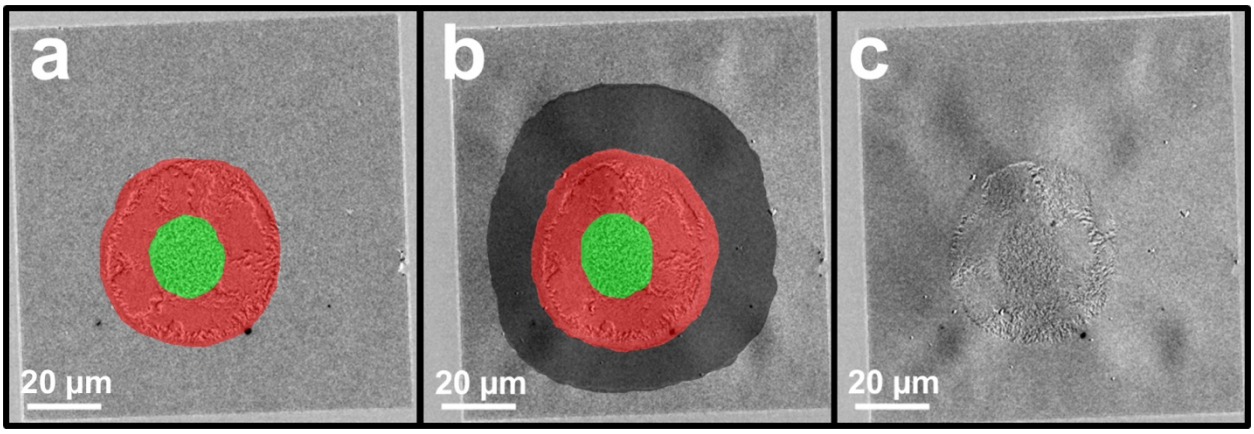

FIG. 2. Fresnel imaging of *in situ* laser-initiated morphological changes and magnetization reversal acquired at 6% objective-lens excitation (90 mT). The false-coloring shows the area of each response. Each panel is a difference image formed by subtracting pre- and post-laser-irradiation Fresnel images. The difference images were acquired at: (a) +35-mm defocus at 0° α-tilt (*i.e.*, at normal incoming-electron incidence); green = densely-nucleated nanocrystalline region, red = sparsely-nucleated region, (b) +35-mm defocus at 20° α-tilt; green = densely-

167 nucleated nanocrystalline region, red = sparsely-nucleated region, black = magnetically-switched
168 region, and (c) +35-mm defocus at 20° α-tilt and after application of a 1.2-T magnetic field
169 oriented perpendicular to the specimen plane. Note the absence of the magnetically-switched
170 region after application of the field.
171
172 Because the Fresnel image in Fig. 2(a) was generated at normal incidence, the observed
173 contrast arises from photothermally-crystallized regions having magnetization directions $(\vec{B})$
174 oriented such that $F_{L,n} = q(\overrightarrow{B_{C,n}} \times \vec{v}) = q\|\overrightarrow{B_{C,n}}\|\|\vec{v}\| \sin\theta_n \neq 0$, where $F_{L,n}$ is the Lorentz force at
175 each of the n photothermally-nucleated single crystals, q is the electron charge, $\overrightarrow{B_{C,n}}$ is the
176 magnetic-field vector of each of the n single crystals, $\vec{v}$ is the fixed electron-velocity vector, and
177 θ_n is the angle formed between $\overrightarrow{B_{C,n}}$ and $\vec{v}$. Further, the varying contrast strength in this region
178 suggests a random crystallite orientation. Consequently, the intrinsic perpendicular component
179 of the pristine (*i.e.*, morphologically unchanged) film $(\overrightarrow{B_P})$ is not seen with this configuration,
180 because the magnetization direction of these regions is oriented such that $\overrightarrow{B_P} \times \vec{v} = 0$. By
181 changing the orientation of the film relative to $\vec{v}$ to non-normal incidence, however, F_L arising
182 from $\overrightarrow{B_P}$ becomes non-zero. In this way, the domain-wall structure in the pristine region –
183 occurring at two oppositely-oriented but perpendicularly-magnetized areas – can be imaged. In
184 the Fresnel image, this appears as an annulus of contrast 10 to 20 μm wide (black) encircling the
185 sparsely-nucleated region (red) [Fig. 2(b)]. After applying a 1.2-T aligning field and then
186 returning to Fresnel-imaging mode, the annulus of contrast is no longer observed, indicating the
187 magnetization in that region is switchable [Fig. 2(c)]. Note that, while somewhat weakened, the
188 contrast strength of the densely- and sparsely-nucleated regions [green and red in Fig. 2(b),

189 respectively] persists after application of the field. This indicates the magnetization is pinned at
190 these sites due to morphological changes in the film.

191 In magneto-optic experiments, there are several laser parameters that can be varied (*e.g.*,
192 repetition rate, pulse energy, and irradiation time), and it is probable that the effects of each
193 individually and taken together will lead to varied reported observations and potentially
194 inconsistent device performance. Fluence is one such parameter that may produce observable
195 threshold-type behavior for switching and also strongly influence the onset of morphological
196 variation. Importantly, previous work on GdFeCo indicates the fluence window is small for
197 helicity-dependent single-pulse switching, suggesting device tolerances based on this concept
198 may be severely limited and mechanisms may be easily convoluted and obscured [18]. Note,
199 however, that this may not be the case in helicity-independent switching (*i.e.*, with linearly-
200 polarized light, as used here). Further, as shown in Fig. 2, deleterious photothermally-induced
201 morphological changes that occur above some specimen-dependent value influence the observed
202 switching behavior. Consequently, in order to determine the effects of laser fluence on thin
203 TbCo films, individual series of 20,000 laser pulses (270 fs) of fixed fluence were delivered in
204 one second (here, referred to as a cycle) *in situ* to a single specimen region at 0% objective-lens
205 excitation (10 mT). It is important to note that the duration of laser irradiation for multiple-pulse
206 magnetization reversal can affect the threshold-fluence value, as demonstrated when comparing
207 the results shown in Fig. 2 (several seconds) and Fig. 3 (one second). A Fresnel image was
208 acquired following each fixed-fluence series, after which the objective-lens excitation was
209 increased such that a 1.2-T field was generated, thus realigning the magnetization vector of still-
210 switchable specimen regions. Following this, the fluence was increased, the next series was
211 delivered, a Fresnel image was acquired, and a 1.2-T field was again applied.

Results of the multiple-pulse fluence-dependent experiment are summarized in Fig. 3. As anticipated, a variety of effects – both reversible and irreversible – were observed to occur in the TbCo films. Specifically, four crystallographically- and/or magnetically-distinct regions developed at discrete fluence values upon increasing from 0 to 26 mJ/cm^2. In the Fresnel images, each region produces a distinct contrast pattern with relatively abrupt transitions separating one from the next, indicating the magnetic behavior of each is also distinct. Stemming from the resulting image contrast following application of an aligning field, the regions are defined as reversible (I) (*i.e.*, the magnetization can be reversed with an applied external field), irreversible (II), completely demagnetized (III), and morphologically damaged (IV). That is, (I) is morphologically unchanged and magnetically switchable, (II) is nucleated and magnetic but no longer switchable, (III) is completely demagnetized and also nucleated but with a different morphology than (II) (discussed below), and (IV) is significantly laser damaged. These distinct behaviors first occurred at approximately 5.7, 9.6, 14, and 22.3 mJ/cm^2. Note that regions (I) and (II) are morphologically and magnetically similar to the laser-irradiated specimen shown in Fig. 2.

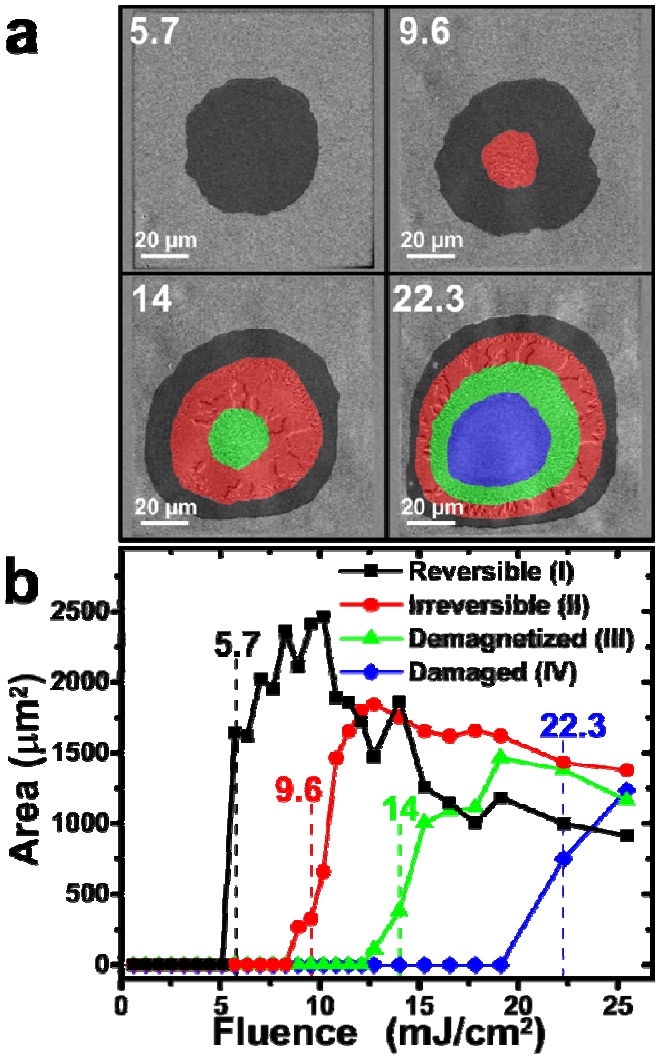

FIG. 3. Laser-fluence dependence of morphological changes and magnetization reversal. (a) Fresnel images acquired at 0% objective-lens excitation (10 mT) after irradiation with the fluences (mJ/cm^2) shown in the upper left of each panel. The false-coloring shows the area of each response, as designated in (b). (b) Image area as a function of incident laser fluence for four distinct specimen responses: (I) reversible (black squares), (II) irreversible (red dots), (III) demagnetized (green triangles), and (IV) damaged (blue diamonds). The panel summarizes the contributions of each response to the overall specimen area across which contrast changes were observed. The analysis method for delineating each of the regions is described in the Supplemental Material [21].

238

239 In addition to exhibiting threshold behavior, each of the four distinct regions shown in
240 Fig. 3 persisted for a finite range of fluences prior to the onset of each subsequent response.
241 Onset of the magnetically-reversible region (I) occurred at 5.7 mJ/cm^2 and persisted to
242 approximately 8.3 mJ/cm^2 prior to the onset of region (II); the film exhibited a completely
243 reversible magnetic response within this relatively small fluence window. Further, no
244 discernible changes were observed in the film after application of each cycle, aside from an
245 increase in the area of the reversible region from approximately 1,700 μm^2 to 2,400 μm^2 [Fig.
246 3(b)]. At 9.6 mJ/cm^2, irreversible (II) structural changes, consisting of sparsely-nucleated
247 crystallites which act as magnetic pinning sites, were first observed at the approximate center of
248 the irradiation pulse train. The area of this region increased with increasing fluence up to 12.1
249 mJ/cm^2, at which point a new morphological and magnetic response was observed. This new
250 region (III, demagnetized) consisted of densely-nucleated crystallites, again centered at the
251 approximate center of the train of pulses having a Gaussian intensity profile. At fluences above
252 approximately 19.1 mJ/cm^2, an additional region (IV, damaged) formed and was devoid of
253 magnetic contrast. Finally, the film ruptured just above 26 mJ/cm^2. As seen in Fig. 3, the
254 boundaries of each of the regions advanced outward from the pulse-train center with increasing
255 fluence, while the measured areas decreased owing to growing contributions by subsequent
256 regions to the signal. Such behavior can likely be attributed mainly to photothermal effects and
257 heat transport properties of the film, though a magnetically reversed region does persist
258 throughout.

259 In order to determine the structural variation across the four distinct regions shown in
260 Fig. 3 (I through IV) and correlate this to the laser-initiated magnetization behavior, spatially-

261 specific parallel-beam selected-area electron diffraction was performed, the results of which are
262 summarized in Fig. 4. As can be seen, the degree of crystallinity decreases while moving
263 outward from the center of the laser-irradiated region [*i.e.*, from region (IV) to (I)],
264 approximately following the Gaussian photothermal profile generated by the pulse train. This is
265 deduced by noting the decrease in both number and sharpness of the Debye-Scherrer rings while
266 moving away from the central region [Fig. 4(b)]. Radially-averaged intensity profiles further
267 reflect the spatial variation in crystalline order [Fig. 4(c)]. The general reduction in peak FWHM
268 indicates the average crystallite size increases while moving from region (I) to (IV), as per the
269 Scherrer equation, while the emergence of new peaks suggests several or all of the specimen
270 components (*i.e.*, substrate, capping layers, and TbCo film) have undergone crystal nucleation
271 and growth [further supported by the disappearance of the prominent diffuse ring observed in
272 (I)]. While specific peak assignments cannot be made with confidence owing to overlap and the
273 presence of multiple species [three elements (Tb, Co, and Ta) and a compound (Si_3N_4)], not all
274 peaks in the profile from region (IV) can be assigned to any single component. Note that the
275 radial profile from region (I) matches that of the pre-irradiated specimen (see Fig. 2) and
276 indicates no morphological change has occurred in this area. Determination of the crystal
277 structures and the hypothesized spatially-dependent composition of the complex photothermally-
278 induced morphology will be the subject of future studies. See the Supplemental Material for
279 high-resolution TEM analysis of the transition area between the sparsely nucleated region (II)
280 and the more heavily nucleated region (III) shown in Fig 4 [21]. It is worth noting that the
281 photothermally-induced crystallization shown in Fig. 4 is qualitatively similar to that reported for
282 dynamic TEM and ultrafast electron microscopy studies of amorphous Ge and TiO_2 [29-32].
283

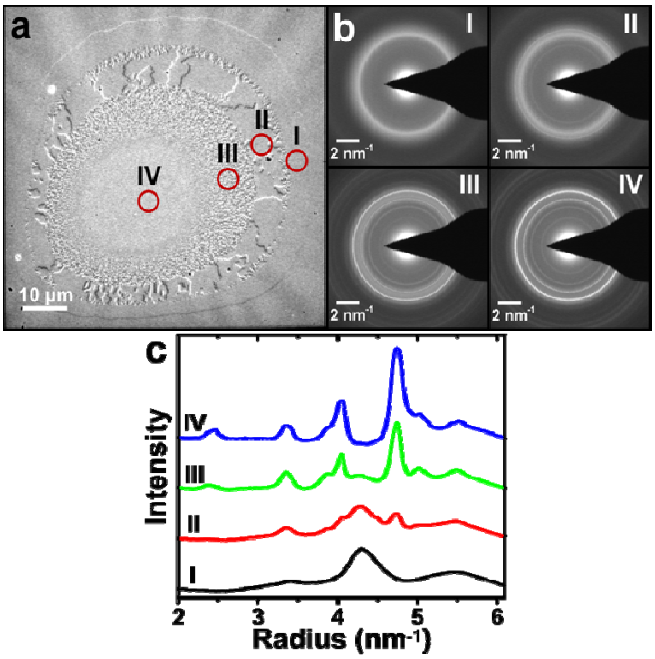

FIG. 4. (a) Fresnel image of the film acquired with 0% objective-lens excitation after irradiation with a train of fs laser pulses. Locations of the distinct regions are denoted by I, II, III, and IV and correspond to the reversible, irreversible, demagnetized, and damaged regions, respectively (see Fig. 3). The red circles indicate the position of the selected-area aperture used to obtain the four diffraction patterns shown in panel (b). (b) Selected-area diffraction patterns of the film obtained from the locations indicated with the red circles in panel (a). The region labels (*e.g.*, IV) are shown in the upper-right corner of each panel. (c) Radially-averaged intensity as a function of radius of the selected-area diffraction patterns shown in panel (b). The approximate center of the patterns corresponds to 0 nm^{-1}. The background has been subtracted and the spectra offset for clarity.

As shown above, onset of the reversible (I) magnetic response for a train of 20,000 laser pulses of 270-fs duration separated by 50 µs each (*i.e.*, one cycle) occurred at 5.7 mJ/cm^2 and persisted up to 8.3 mJ/cm^2. Above this fluence, the irreversible (II) response was first observed.

While one could argue that the reversible (I) and irreversible (II) responses observed here using Fresnel TEM correlate well with the helicity-independent switching and the multi-domain state, respectively, observed using optical techniques [32], it is important to note that switching could also be induced photothermally, as discussed below. Increased crystallinity in (II) compared to (I), as reflected in the selected-area diffraction patterns [Fig. 4(b)], suggests that the laser-induced formation of small crystal grains measuring tens of nanometers during MOKE measurements could be misidentified as a multi-domain state owing to limits in spatial resolution and lack of *in situ* structural characterization capabilities in such all-optical methods. That is, the formation of small crystallites that pin magnetic response could go unnoticed. Further, studies that investigate the effects of laser irradiation often employ a multiple-pulse approach for initiating an apparent magnetic response [5,6,20,34]. Thus, generation of a clear picture of pulse-to-pulse effects on specimen morphology and magnetism would be informative.

Because a train of laser pulses can lead to deleterious morphological variations in the films over a relatively small span of fluences, as shown here, the delicate interplay of fluence, number of pulses, and duration between each must be carefully determined within regions (I) and (II). Consequently, the result of delivering an increasing number of laser cycles, where one cycle = 20,000 pulses and each pulse is of 5.7-mJ/cm^2 fluence [*i.e.*, the threshold fluence necessary to induce a reversible magnetic response at these laser parameters; see Fig. 3(b)], is shown in Fig. 5(a). Between each cycle, the magnetization direction was reset via objective-lens excitation to 88% (1.2 T). Note that even at the threshold fluence for the magnetization reversal at these laser settings, the formation of irreversible regions (*i.e.*, no longer magnetically switchable) occurred after application of only 16 cycles. Further, continued application increased the relative area of the irreversible region, reaching nearly 50% after 500 cycles. That is, while the total response

area remained approximately unchanged, the ratio of irreversible to reversible area steadily increased from zero at up to 16 cycles to nearly 0.5 after 500 cycles. Thus, even at the minimum fluence needed to induce a multi-pulse reversible magnetic response for these laser parameters, deleterious morphological variations occurred after application of less than 20 cycles. To further expand on the laser-initiated effects on the TbCo film, single-pulse magnetization switching was investigated.

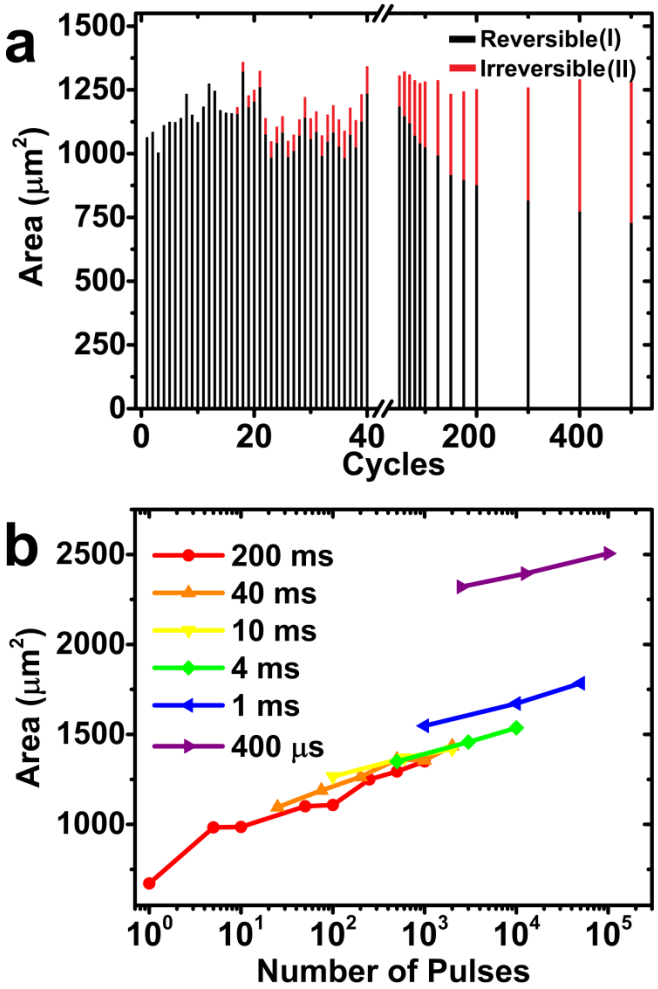

FIG. 5. Effect of number of laser-irradiation cycles, number of individual fs pulses, and duration between each pulse on morphology and robustness of magnetization reversal in TbCo. (a) Area of the reversible (I, black) and irreversible (II, red) responses as a function of the number of

333 incident laser-pulse cycles (1 cycle = 20,000 pulses delivered over 1 second; fluence = 5.7
334 mJ/cm^2), as determined from Fresnel images obtained at 0% objective-lens excitation (10 mT).
335 Note that the scale changes from increments of 20 to 200 cycles at the break in the *x*-axis. (b)
336 Area of the reversible magnetic-response region (I) induced by individual fs laser pulses at the
337 minimum fluence for single-pulse switching (15.5 mJ/cm^2) as a function of the number of pulses
338 (log scale) and time between each (different colors and symbols; *e.g.*, τ = 200 ms denoted by red
339 circles) obtained from Fresnel images of the film acquired with 6% objective-lens excitation (90
340 mT).
341
342 The effects of individual fs laser pulses, delivered at the experimentally-determined
343 minimum-fluence threshold for observable single-pulse switching, on the size and behavior of
344 the reversible, laser-initiated magnetic response [*i.e.*, region (I)] are shown in Fig. 5(b). Here,
345 changes in the area of the response were determined as a function of both the number of
346 individual pulses applied (*x*-axis) and the duration between each (colors and symbols) at the
347 minimum fluence (15.5 mJ/cm^2) needed to produce magnetization reversal. The duration
348 between pulses (τ) was controlled by pulse picking with an electro-optic modulator. In this way,
349 the pulse energy – and thus the fluence (15.5 mJ/cm^2) – were fixed providing a means to
350 investigate the maximum single-pulse switching frequency capable for this film structure before
351 the onset of laser-induced morphological changes. After delivery of each series of pulses, the
352 objective-lens excitation was increased to 88% (1.2 T), thus re-aligning the film magnetization
353 direction prior to the next experiment. Here, it is noted that the single-pulse switching was not
354 able to be reversed with each pulse as demonstrated in other techniques. It is hypothesized that
355 this is due to the stray magnetic field applied parallel to the film normal originating from the

356 objective lens of the TEM. Indeed, recent work on GdFe has shown that an opposing magnetic
357 field can cause laser-induced switching to become unstable, with a return to its original state
358 upon cessation of irradiation [35]. Though a specific mechanism for the observed switching is
359 not assigned here, results of preliminary photothermal modeling of the multilayer, freestanding,
360 thin-film specimen indicate the temperature rise could exceed the measured 455 ºC
361 compensation temperature (see the Supplemental Material) resulting in a heat-assisted
362 compensation-point reversal [10,21].

363 The single-pulse switching data in Fig. 5(b) are displayed in such a way as to
364 simultaneously convey several notable observations. First, the overall size of the reversible
365 response area gradually increased with increasing number of applied pulses at a specific value of
366 τ (*e.g.*, 200 ms). Second, reversible, laser-initiated magnetization switching was observed for
367 application of up to 10^5 individual pulses and for τ ranging from 200 ms down to 400 μs (note
368 that relatively small areas of irreversible damage were observed beginning at $\tau = 200$ μs). Third,
369 overall larger reversible regions were observed at smaller values of τ, but only for durations
370 below 4 ms. That is, the total response area dramatically increased for $\tau < 4$ ms (*e.g.*, $\tau = 400$ μs
371 compared to 1 ms) for the same number of pulses delivered to the film. At 4 ms and above, the
372 response area is the same size for irradiation with (for example) 10^3 pulses.

373 Taken as a whole, these observations can be rationalized by noting the expected interplay
374 of accumulation of photothermal energy in the film, the development of a thermal gradient, and
375 the effects on spin transport. For a particular pulse-series set of a specific τ [*e.g.*, from one to 10^3
376 pulses per series, $\tau = 200$ ms; red dots in Fig. 5(b)], the gradual increase in response area is
377 attributed to the manner in which electron current and spin behave with respect to thermal
378 gradients. For example, magnons traveling down the thermal gradient produced by the laser-

379 pulse train (*i.e.*, radially away from the center of the irradiated region) generate a torque at the
380 domain wall [36]. This interaction results in domain-wall motion outward along a trajectory
381 parallel to the path of the radially-propagating magnon, thus increasing the size of the response
382 area with each delivered pulse. The spin Seebeck effect, in which a thermal gradient generates a
383 voltage that drives electron spin, may also manifest as domain-wall motion in the *in situ* Fresnel
384 images [37,38]. These mechanisms for relatively gradual expansion of the response area are
385 convoluted with that due to rapid accumulation of thermal energy in the film, which manifests at
386 values of τ below 4 ms. At shorter pulse-to-pulse durations, increasing volume of the specimen
387 will experience a temperature rise above the thermal switching threshold, thus increasing the
388 observed response area beyond that expected from the more gradual mechanism due to magnon
389 generation and propagation.
390

391 **CONCLUSIONS**

392 In conclusion, it has been shown here that, with *in situ* Fresnel imaging in a modified
393 TEM, the correlated effects of both multiple-pulse and single-pulse laser-initiated magnetic-
394 switching behavior and photothermal morphological variations can be directly visualized,
395 deconvoluted, and quantified as a function of a variety of fs-pulse parameters. These results
396 provide evidence that deleterious morphological variations can arise during these experiments,
397 the structural effects of which can influence both the local and global magnetic behavior of thin
398 films of RE-TM ferrimagnetic alloys. Indeed, proper isolation and characterization of such
399 photothermally-induced structural changes is critical to developing a comprehensive and
400 accurate description of the processes contributing to magneto-optic and heat-assisted
401 phenomena, and thus is vital to robust device performance. Future studies with the above-

402 described methods will focus on quantifying equilibrium and non-equilibrium photothermal
403 profiles, characterizing the nucleated film to quantify the structures formed, and further,
404 resolving the domain-wall dynamics arising during fs magnetization reversal – via stroboscopic
405 ultrafast electron microscopy [23,27,39-41] – and directly imaging the associated thermal energy
406 generation and propagation and resolving its effect on the magnetic and spin-transport behavior
407 of the film [42].
408

409 **ACKNOWLEDGMENTS**

410 This work was supported partially by the National Science Foundation through the University of
411 Minnesota MRSEC under Award Number DMR-1420013. Part of this work was carried out in
412 the College of Science and Engineering Characterization Facility, University of Minnesota,
413 which has received capital equipment funding from the NSF through the UMN MRSEC program
414 under Award Numbers DMR-0819885 and DMR-1420013. Part of this work was carried out in
415 the College of Science and Engineering Institute for Rock Magnetism, University of Minnesota,
416 which is made possible in part through the Instrumentation and Facilities program of the NSF
417 Earth Science Division. This work was partially supported by C-SPIN, one of six STARnet
418 Centers, a Semiconductor Research Corporation program, sponsored by MARCO and DARPA.
419 Additional support was provided by 3M through a Nontenured Faculty Award under Award
420 Number 13673369 and by the Arnold and Mabel Beckman Foundation through a Beckman
421 Young Investigator Award (D.J.F.). Acknowledgment is made to the Donors of the American
422 Chemical Society Petroleum Research Fund for partial support of this research under Award
423 Number 53116-DNI7.
424

REFERENCES

[1] A. Kirilyuk, A. V. Kimel, and Th. Rasing, Rev. Mod. Phys. **82**, 2731 (2010).

[2] A. Kirilyuk, A. V. Kimel, and Th. Rasing, Rep. Prog. Phys. **76**, 026501 (2013).

[3] A. Hoffmann and S. D. Bader, Phys. Rev. Appl. **4,** 047001 (2015).

[4] C. Stanciu, F. Hansteen, A. Kimel, A. Kirilyuk, A. Tsukamoto, A. Itoh, and Th. Rasing, Phys. Rev. Lett. **99**, 047601 (2007).

[5] C. H. Lambert, S. Mangin, C. S. Varaprasad, Y. K. Takahashi, M. Hehn, M. Cinchetti, G. Malinowski, K. Hono, Y. Fainman, M. Aeschlimann, and E. E. Fullerton, Science **345**, 1337 (2014).

[6] S. Mangin, M. Gottwald, C. H. Lambert, D. Steil, V. Uhlir, L. Pang, M. Hehn, S. Alebrand, M. Cinchetti, G. Malinowski, Y. Fainman, M. Aeschlimann, and E. E. Fullerton, Nat. Mater. **13**, 286 (2014).

[7] M. R. Shcherbakov, P. P. Vabishchevich, A. S. Shorokhov, K. E. Chong, D.-Y. Choi, I. Staude, A. E. Miroshnichenko, D. N. Neshev, A. A. Fedyanin, and Y. S. Kivshar, Nano Lett. **15**, 6985 (2015).

[8] L. He, J.-Y. Chen, J.-P. Wang, and M. Li, Appl. Phys. Lett. **107**, 102402 (2015).

[9] M. Aeschlimann, A. Vaterlaus, M. Lutz, M. Stampanoni, F. Meier, and H. C. Siegmann, Appl. Phys. Lett. **59**, 2189 (1991).

[10] C. D. Stanciu, A. Tsukamoto, A. V. Kimel, F. Hansteen, A. Kirilyuk, A. Itoh, and Th. Rasing, Phys. Rev. Lett. **99**, 217204 (2007).

[11] I. Radu, K. Vahaplar, C. Stamm, T. Kachel, N. Pontius, H. A. Dürr, T. A. Ostler, J. Barker, R. F. L. Evans, R. W. Chantrell, A. Tsukamoto, A. Itoh, A. Kirilyuk, Th. Rasing, and A. V. Kimel, Nature **472**, 205 (2011).

[12] M. H. Kryder, E. C. Gage, T. W. McDaniel, W. A. Challener, R. E. Rottmayer, G. Ju, Y.-T. Hsia, and M. F. Erden, Proc. IEEE **96**, 1810 (2008).

[13] A. V. Kimel, Nat. Mater. **13**, 225 (2014).

[14] E. Beaurepaire, J. C. Merle, A. Daunois, and J. Y. Bigot, Phys. Rev. Lett. **76**, 4250 (1996).

[15] L. Gierster, L. Pape, A. A. Ünal, F. Radu, and F. Kronast, Ultramicroscopy **159**, 508 (2015).

[16] L. Le Guyader, M. Savoini, S. El Moussaoui, M. Buzzi, A. Tsukamoto, A. Itoh, A. Kirilyuk, T. Rasing, A. V. Kimel, and F. Nolting, Nat. Commun. **6**, 5839 (2015).

[17] C. E. Graves, A. H. Reid, T. Wang, B. Wu, S. de Jong, K. Vahaplar, I. Radu, D. P. Bernstein, M. Messerschmidt, L. Müller, R. Coffee, M. Bionta, S. W. Epp, R. Hartmann, N. Kimmel, G. Hauser, A. Hartmann, P. Holl, H. Gorke, J. H. Mentink, A. Tsukamoto, A. Fognini, J. J. Turner, W. F. Schlotter, D. Rolles, H. Soltau, L. Strüder, Y. Acremann, A. V. Kimel, A. Kirilyuk, Th. Rasing, J. Stöhr, A. O. Scherz, and H. A. Dürr, Nat. Mater. **12**, 293 (2013).

[18] A. R. Khorsand, M. Savoini, A. Kirilyuk, A. V. Kimel, A. Tsukamoto, A. Itoh, and Th. Rasing, Phys. Rev. Lett. **108**, 127205 (2012).

[19] U. Bierbrauer, S. Alebrand, M. Hehn, M. Gottwald, D. Steil, D. Lacour, E. E. Fullerton, S. Mangin, M. Cinchetti, and M. Aeschlimann, in *Ultrafast Magnetism I*, edited by J. Y. Bigot, W. Hubner, Th. Rasing and R. Chantrell (Springer, Cham, 2015), Vol. 159, p. 244.

[20] S. Alebrand, M. Gottwald, M. Hehn, D. Steil, M. Cinchetti, D. Lacour, E. E. Fullerton, M. Aeschlimann, and S. Mangin, Appl. Phys. Lett. **101**, 162408 (2012).

[21] See Supplemental Material at [URL will be inserted by publisher] for additional experimental details and characterization data.

[22] C. Phatak, A. K. Petford-Long, and M. De Graef, Curr. Opin. Solid State Mater. Sci. **20**, 107 (2016).

[23] H. S. Park, J. S. Baskin, and A. H. Zewail, Nano Lett. **10**, 3796 (2010).

[24] J. G. Gatzmann, T. Eggebrecht, A. Feist, V. Zbarsky, M. Münzenberg, C. Ropers, and S. Schäfer, Microsc. Microanal. **20**, 1578 (2014).

[25] J. Rajeswari, P. Huang, G. F. Mancini, Y. Murooka, T. Latychevskaia, D. McGrouther, M. Cantoni, E. Baldini, J. S. White, A. Magrez, T. Giamarchi, H. M. Rønnow, and F. Carbone, Proc. Natl. Acad. Sci. U.S.A. **112**, 14212 (2015).

[26] S. P. Weathersby, G. Brown, M. Centurion, T. F. Chase, R. Coffee, J. Corbett, J. P. Eichner, J. C. Frisch, A. R. Fry, M. Guhr, N. Hartmann, C. Hast, R. Hettel, R. K. Jobe, E. N. Jongewaard, J. R. Lewandowski, R. K. Li, A. M. Lindenberg, I. Makasyuk, J. E. May, D. McCormick, M. N. Nguyen, A. H. Reid, X. Shen, K. Sokolowski-Tinten, T. Vecchione, S. L. Vetter, J. Wu, J. Yang, H. A. Dürr, and X. J. Wang, Rev. Sci. Instrum. **86**, 073702 (2015).

[27] J. Qiu, G. Ha, C. Jing, S. V. Baryshev, B. W. Reed, J. W. Lau, and Y. Zhu, Ultramicroscopy **161**, 130 (2016).

[28] T.-M. Liu, T. Wang, A. H. Reid, M. Savoini, X. Wu, B. Koene, P. Granitzka, C. E. Graves, D. J. Higley, Z. Chen, G. Razinskas, M. Hantschmann, A. Scherz, J. Stöhr, A. Tsukamoto, B. Hecht, A. V. Kimel, A. Kirilyuk, Th. Rasing, and H. A. Dürr, Nano Lett. **15**, 6862 (2015).

[29] O. Bostanjoglo, W. Marine, and P. Thomsen-Schmidt, Appl. Surf. Sci. **54**, 302 (1992).

[30] L. Nikolova, T. LaGrange, M. J. Stern, J. M. MacLeod, B. W. Reed, H. Ibrahim, G. H. Campbell, F. Rosei, and B. J. Siwick. Phys. Rev. B **87**, 064105 (2013).

[31] T. T. Li, L. B. Bayu Aji, T. W. Heo, M. K. Santala, S. O. Kucheyev, and G. H. Campbell, Appl. Phys. Lett. **108**, 221906 (2016).

[32] B.-K. Yoo, O.-H. Kwon, H. Liu, J. Tang, and A. H. Zewail, Nat. Commun. **6**, 8639 (2015).

[33] K. Vahaplar, A. M. Kalashnikova, A. V. Kimel, S. Gerlach, D. Hinzke, U. Nowak, R. Chantrell, A. Tsukamoto, A. Itoh, A. Kirilyuk, and Th. Rasing, Phys. Rev. B **85**, 104402 (2012).

[34] A. Hassdenteufel, B. Hebler, C. Schubert, A. Liebig, M. Teich, M. Helm, M. Aeschlimann, M. Albrecht, and R. Bratschitsch, Adv. Mater. **25**, 3122 (2013).

[35] L. Le Guyader, S. El Moussaoui, M. Buzzi, M. Savoini, A. Tsukamoto, A. Itoh, A. Kirilyuk, Th. Rasing, F. Nolting, and A. V. Kimel, Phys. Rev. B **93**, 134402 (2016).

[36] X.-g. Wang, G.-h. Guo, Y.-z. Nie, G.-f. Zhang, and Z.-x. Li, Phys. Rev. B **86**, 054445 (2012).

[37] K. Uchida, S. Takahashi, K. Harii, J. Ieda, W. Koshibae, K. Ando, S. Maekawa, and E. Saitoh, Nature **455**, 778 (2008).

[38] G.-M. Choi, C.-H. Moon, B.-C. Min, K.-J. Lee, and D. G. Cahill, Nat. Phys. **11**, 576 (2015).

[39] A. H. Zewail, Science **328**, 187 (2010).

[40] L. Piazza, D. J. Masiel, T. LaGrange, B. W. Reed, B. Barwick, and F. Carbone, Chem. Phys. **423**, 79 (2013).

[41] D. A. Plemmons, P. K. Suri, and D. J. Flannigan, Chem. Mater. **27**, 3178 (2015).

[42] D. R. Cremons, D. A. Plemmons, D. J. Flannigan, Nat. Commun. **7**, 11230 (2016).